Different Time Scales in the Dissociation Dynamics of Core-Excited CF_4 by Two Internal Clocks

H. Iwayama,[1] C. Léonard,[2] F. Le Quéré,[2] S. Carniato,[3] R. Guillemin,[3] M. Simon,[3] M. N. Piancastelli,[3,4] and E. Shigemasa[1]
[1]*UVSOR Synchrotron Facility, Institute for Molecular Science, Okazaki 444-8585, Japan*
[2]*Laboratoire Modélisation et Simulation Multi Echelle UMR 8208 CNRS, Université Paris-Est Marne-la-Vallée, F-77454 Marne-la-Vallée, France*
[3]*Sorbonne Universités, UPMC Univ Paris 6, CNRS, UMR 7614, Laboratoire de Chimie Physique-Matière et Rayonnement, F-75005 Paris, France*
[4]*Department of Physics and Astronomy, Uppsala University, SE-75120 Uppsala, Sweden*
(Received 17 February 2017; revised manuscript received 13 June 2017; published 15 November 2017)

Fragmentation processes following C $1s \rightarrow$ lowest unoccupied molecular orbital core excitations in CF_4 have been analyzed on the ground of the angular distribution of the CF_3^+ emitted fragments by means of Auger electron-photoion coincidences. Different time scales have been enlightened, which correspond to either ultrafast fragmentation, on the few-femtosecond scale, where the molecule has no time to rotate and the fragments are emitted according to the maintained orientation of the core-excited species, or dissociation after resonant Auger decay, where the molecule still keeps some memory of the excitation process before reassuming random orientation. Potential energy surfaces of the ground, core-excited, and final states have been calculated at the *ab initio* level, which show the dissociative nature of the neutral excited state, leading to ultrafast dissociation, as well as the also dissociative nature of some of the final ionic states reached after resonant Auger decay, yielding the same fragments on a much longer time scale.

DOI: 10.1103/PhysRevLett.119.203203

Following core excitation, the relaxation pathway of a molecular system might involve complex fragmentation patterns, depending upon the nature (bound or dissociative) of the core-excited state and/or of the final states reached during the relaxation process. In particular, in many systems elongation and breaking of chemical bonds can occur during the lifetime of the excited state: in this case, the dissociation is defined as ultrafast, since typical lifetimes of core-excited states in molecules containing light atoms are of the order of few femtoseconds (see, e.g., Refs. [1–10]). Molecular fragmentation can also occur in a final state reached after resonant Auger decay, if such a final state is unstable. In this case, the time scale for the breaking of the chemical bond is much longer.

The competition between electronic decay and fragmentation in molecules was reported already in the literature (see, e.g., the seminal papers [11–13] on HCl, DCl, Cl_2, and HF). Ultrafast phenomena can be identified by means of their clear signature in the resonant Auger spectra, which exhibit two types of well-separated lines: together with the spectral features of the molecular final states, extra peaks related to fragments are present, and can be assigned on the ground of their dispersion law [4–8,11–13]. This is the basis of the so-called core-hole clock method, which allows characterizing ultrafast phenomena with an "internal clock," the core-hole lifetime, rather than by the use of a time-resolved source [1–3].

While ultrafast dissociation is possible during the core-hole lifetime and can be detected in the resonant Auger spectra, dissociation on a longer time scale, and, namely, after a final state is reached which can in turn be dissociative, does not yield a clear signature in the decay spectra, because the fragment spectral patterns cannot be detected.

A direct comparison between pathways leading to the same fragmentation products, but of a different nature, and, in particular, with very different time scales, has not yet been attempted, which is the heart of the present work.

Here we examine a prototypical system for fast relaxation dynamics, and, namely, CF_4. This molecule is known to undergo ultrafast fragmentation yielding the excited C^*F_3 species after C $1s$ core excitation to the LUMO (lowest unoccupied molecular orbital). We have already reported such fragmentation pattern [14]. Resonant Auger-ion coincidences for this system have been published [15]. However, the relaxation process of CF_4 is rather complex, because fragmentation is possible not only due to the dissociative nature of the intermediate core-excited state, but also because some of the ionic final states reached after resonant Auger decay are in turn dissociative.

A crucial point is that although the produced charged fragment CF_3^+ is the same in both cases, these two dissociation patterns are very different, due to their different time scale. In particular, the angular distribution of the ejected fragment reflects the time scale of the bond breaking: if the bond rupture occurs during the core-hole lifetime, the molecules are still oriented along the direction of the electric field vector, and the fragments are ejected in a

very directional manner, while if the dissociation takes place in the final states it takes much longer times, the molecular ions have time to rotate and to reach a random distribution, and the ejection of the fragments is rather isotropic. However, we will show in the following discussion that some "memory" of the orientation induced by primary excitation can remain.

While there is a rather large literature describing ultrafast dissociation enlightened in resonant Auger spectra, there is no analogous bulk of works on angular distribution of fragments.

In a previous paper [16], photoion imaging for CF_3^+ ions produced after valence ionization of CF_4 was reported, and found that for some of the photon energies used the distribution was not isotropic. This finding was related to the populations of excited states with symmetry lower than the T_d symmetry group of the CF_4 ground state. Similar observations were reported in another paper [17] by threshold photoelectron-photoion imaging measurements. However, the time scales and the wave-packet dynamics of the processes were not discussed in either work.

We performed resonant Auger electron-ion coincidence measurements, which allowed us to enlighten the angular distribution of the fragments, which is very different according to the time scale of photodissociation.

In particular, fragments emitted during the core-hole lifetime possess a directional angular distribution, since the molecule is oriented by the primary excitation process with one of the C—F bonds along the $\bar{E}$ vector, and has no time to rotate during few femtoseconds.

At variance with that, when dissociation occurs after an unstable final state is reached following Auger decay, it takes much longer time, and the molecule can reassume a random distribution, which can lead to an isotropic distribution of the emitted fragments. However, we were able to detect some subtle differences between the fragmentation patterns for a specific final state on resonance and off resonance, hinting at the molecule keeping some "memory" of the excitation process.

The experiments were performed on the soft x-ray beam line BL6U at UVSOR Synchrotron Facility, Okazaki, Japan. The radiation from an undulator was monochromatized by a variable-included-angle varied-line spacing plane-grazing monochromator. The photon energy of 298.4 eV was used for C 1s-to-LUMO core excitations, and the photon energy resolving power was set to 10 000. The polarization vector was horizontal. To estimate off-resonant photoionization contributions, we also conducted measurements at photon energy of 296.4 eV. The monochromatized radiation was introduced into a cell with sample gases.

The experimental setup for Auger electron-photoion coincidence (AEPICO) measurements comprised a double toroidal electron analyzer and an ion momentum spectrometer, each of which is equipped with time- and position-sensitive detectors. Full details of its design and operation are described elsewhere [18,19].

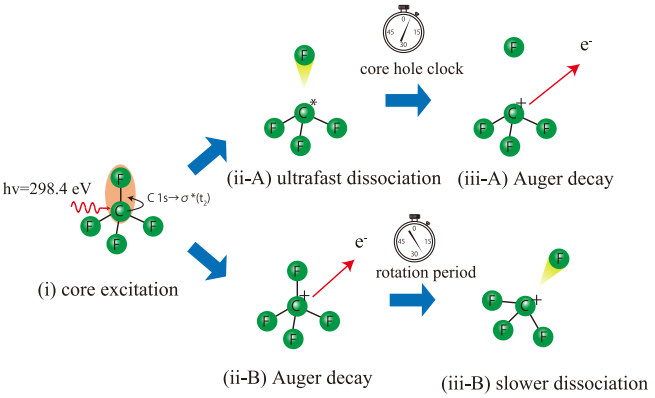

FIG. 1. Top: schematic of core excitation followed by ultrafast dissociation and resonant Auger emission from the fragment. Bottom: schematics of resonant Auger decay in the molecule followed by dissociation in the molecular ion.

In Fig. 1 we show a cartoon of the two different processes leading to the same fragment CF_3^+, one on the time scale of a few femtoseconds, the other one on a much longer one. High-resolution resonant Auger spectra and their detailed assignment are reported in Ref. [14]. Here we concentrate on Auger electron-photoion coincidence measurements with sufficient electron kinetic energy resolution to identify the various features in the decay spectrum.

In Fig. 2, top, red line, we show the energy position of the resonant Auger electrons emitted after C 1s → LUMO excitation on a binding energy scale. In our previous paper [14], we were able to identify the spectral features as related to the intact molecular ion CF_4^+ or to the CF_3^+ fragment on the ground of their dispersion law. The filled red spectrum shows coincidence measurements of resonant Auger electrons and CF_3^+ ions.

The electron kinetic energies of peak labeled area A in the figure correspond to the resonant Auger decay of the C^*F_3 fragment originated from ultrafast dissociation, while the electron energy of the peak labeled area B is related to a molecular CF_4^+ final state, namely, the $3t_2^{-1}$ one [14].

This is the first indication that CF_3^+ is produced in two different photodissociation channels.

In Fig. 2, bottom, we report the angular distribution of the CF_3^+ fragments in coincidence with electrons of the area A (left panel), and of the area B (right panel). The direction of the $\bar{E}$ vector is vertical in both cases.

In both lower and upper panels the contribution of direct photoemission has been eliminated by subtracting spectra taken off resonance. Such contribution does not exist for area A, which appears only on resonance. For area B, the line shape is very different on and off resonance (see Ref. [14]). In particular, it is distorted by the nuclear motion due to the wave packet evolving along the potential energy

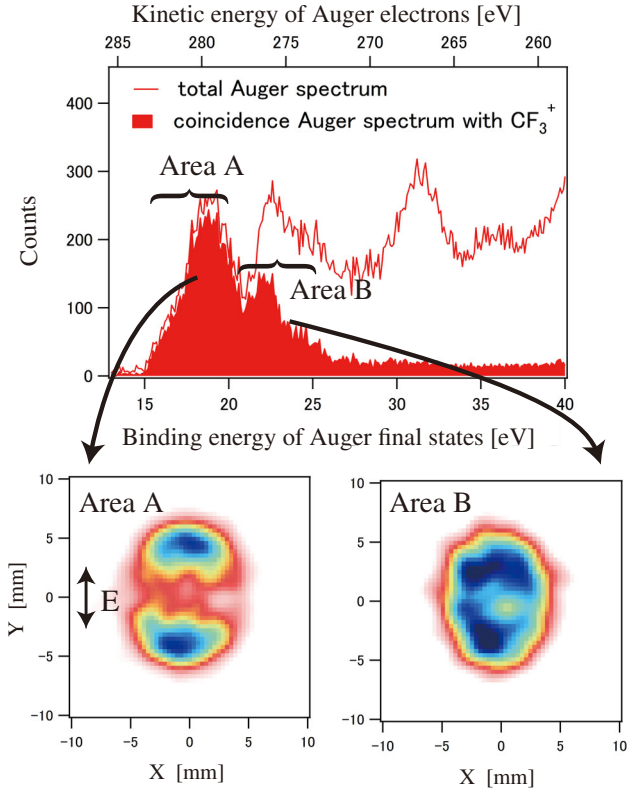

FIG. 2. Top, red line: resonant Auger spectrum after C $1s \rightarrow$ LUMO excitation; solid red area: coincidences between the resonant Auger electrons and the CF_3^+ ion. Bottom: angular distribution of the CF_3^+ fragments in coincidence with the electrons emitted in the resonant Auger decay of the fragment (left panel) and in a molecular resonant Auger decay (right panel). The direction of the $\bar{E}$ vector is indicated.

surfaces. Therefore, we assume that a possible interference between direct and resonant contributions is negligible.

We can immediately visualize that in case of ultrafast fragmentation (left panel) the angular distribution of the CF_3^+ fragments is very asymmetric and peaked along the direction of the $\bar{E}$ vector, while in the case of CF_3^+ yield after resonant Auger decay reaching the $3t_2^{-1}$ final state the angular distribution of the fragments is much more isotropic.

Such large difference is due to the very different time scales of the two fragmentation processes. The molecule is oriented by the primary excitation with the $\bar{E}$ vector along the direction of one of the C—F bonds. If the CF_3^+ fragment is produced during the lifetime of the core-excited state, which is of about a few fs, the molecule has no time to rotate. If the dissociation takes place after one of the molecular final states is reached following resonant Auger decay in the intact molecule, in principle the process takes a much longer time, the molecule has time to rotate, can "forget" the direction of the excitation, and the C—F bond breaking does not occur preferentially along the direction of the $\bar{E}$ vector, but it is rather isotropic.

However, by a closer look, we notice that the distribution even for area B is not completely isotropic. This finding is confirmed by the angular distributions of the fragments (β values), which are 1.1 ± 0.1 for area A and 0.4 ± 0.1 for area B, obtained by fitting the angular distributions with the standard β formula [16].

While the fragment angular distribution can immediately give a qualitative description on the dissociation taking place during core-hole lifetime or later, a deeper assessment on the different time scales is needed, which can be derived from suitable theoretical work.

In order to describe the potential energy surfaces of all ground, intermediate and final states involved, and to obtain a quantitative evaluation of the dynamics of the different fragmentation processes, *ab initio* calculations were performed. The technical details are described in Ref. [20]. The resulting curves have been plotted along the C—F bond distance in Fig. 3 with the definition of the dissociation limits at large distances. On the bottom, we show the electronic ground state potential curve of CF_4. On the middle, the lower CF_4^+ final states are displayed. The black curves correspond to the $3t_2^{-1}$ final state, for which we have shown in a previous publication that we can observe resonant enhancement. The three degenerate electronic components in T_d symmetry split into one $^2A_1$ and one ^2E states in C_s symmetry when the C—F bond length is stretched. These two states present barrier to dissociation

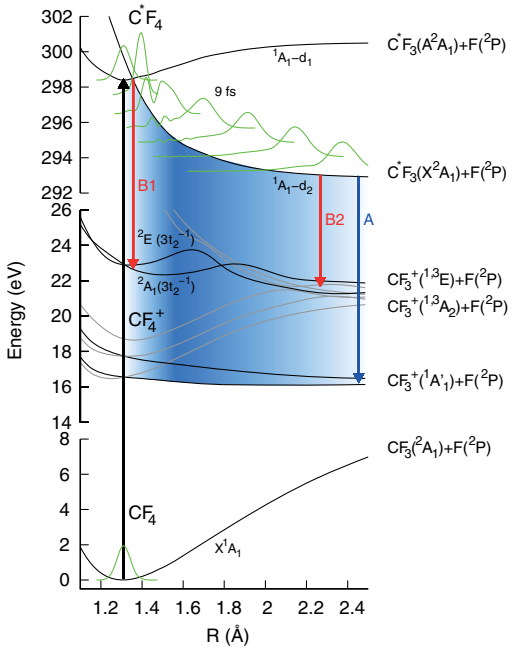

FIG. 3. Potential curves along the $R =$ C—F bond distance of the ground, intermediate and final states in CF_4. The time step between the different wave-packet plots is 3 fs. Grayed potentials are not directly involved in the studied process. The first two electronic states of C^*F_4 have been quasidiabatized. All other electronic states are adiabatic. The shaded area represents the decay probability in the fragment (A process) (see text).

towards the third limit due to avoided crossing with higher excited states. The lower-lying valence states do not show a relevant effect on resonance and are plotted in gray. The top part of Fig. 3 corresponds to the two lowest electronic states of the core-excited C^*F_4 species.

In order to estimate the C—F bond elongation during the Auger process, wave-packet propagation was performed. The first step of the experimental process consists in the vertical excitation of the vibrational ground wave packet of the X^1A electronic ground state of CF_4 to C^*F_4. The electronic ground state X^1A_1 of C^*F_4 is interacting with a second $^1A_1$ electronic state. As a consequence, an avoided crossing occurs in the Franck-Condon region. We performed a quasidiabatization of both electronic components in order to provide potential energy surfaces suitable for the quantum dynamic step. The resulting diabatized potential energy curves, $^1A_1$-d_1 and $^1A_1$-d_2, are depicted in Fig. 3. The $^1A_1$-d_1 state is bound and dissociates towards the second asymptote and $^1A_1$-d_2 is purely dissociative, and dissociate towards the first asymptote. They cross at $R_{C-F} = 1.35$ Å, close to the equilibrium position of the bound state.

The wave packet was then set on the bound $^1A_1$-d_1 state and propagated. Because of the diabatic coupling term, part of the wave packet goes in the dissociative channel whose population increases to 0.9 after 10 fs. Figure 3 shows schematic snapshots of the wave packet every 3 fs and it is clear from this propagation rate that a significant part of the C^*F_4 molecules can extend their dissociative CF bond to reach the $C^*F_3 + F$ before Auger decay since the C_{1s} core-hole lifetime of CF_4 has been evaluated at 8.5 fs [28].

From this observation we can derive an interpretation of the angular distribution of the CF_3^+ fragments of Fig. 2.

As mentioned above, the area A angular distribution suggests an Auger decay from the C^*F_3 fragment. Experiments have also shown that it corresponds to decays from the C^*F_3 fragment, produced by the fraction of molecules which undergo C—F bond breaking within the core-hole lifetime of 8.5 fs [14]. Figure 3 shows that, after 18 fs, more than 20% of the molecules not yet decayed have one of their C—F bond distance increased by 1 Å. We can consider this position, labeled A in Fig. 3, as an asymptotic value in the wave-packet evolution, and leading to the $CF_3^+(^1A_1') + F$ dissociation channel. However, during the core-hole lifetime (8.5 fs) a relevant fraction of excited molecules undergo C—F bond breaking, or at least a large elongation of one C—F bond, and subsequent Auger decay in the C^*F_3 fragment, accounting for the peak A in the decay spectrum. The shaded area in Fig. 3 indicates that such decays can take place in a continuous way down to times much shorter than the marked asymptotic value. This process is very fast compared to the estimated rotational period of tetrahedral CF_4 which can be evaluated at 300 fs from Boltzmann rotational distribution at 300 K.

In Fig. 3, since the potentials involved here follow a parallel evolution along C—F and are already quite flat at $R_{C-F} = 2.4$ Å, the transition energy should be close to the asymptotic energy difference of 277 eV. However, our model considers a fixed tetrahedral geometry for the CF_3 fragment. Taking into account the deformation of CF_3 from tetrahedral to planar during dissociation, increases the asymptotic transition energy by 2.6 eV, and we expect the exact value of transition energies to be very close to the 280 eV, maximum of area A in Fig. 2. The vibrational excitation by kinetic energy reconversion of CF_3^+ can play a role in the transition energy and was suggested experimentally [14] to be at the origin of the broad area A peak of Fig. 2.

The area B angular distribution may result from two different processes labeled $B1$ and $B2$ on Fig. 3, involving the $3t_2^{-1}$ electronic components of CF_4^+. Although the final states are the same, we can distinguish between "faster" and "slower" Auger decay processes.

The $B1$ process corresponds to a fast (<9 fs) Auger decay from the C^*F_4 region to $3t_2^{-1}$ in tetrahedral geometry. This final state splits into ^2E and $^2A_1$ electronic components. The potential wells in these states each supports six vibrational states which may eventually dissociate via tunneling but with lifetimes computed from a Prony analysis of wave-packet autocorrelation functions [29], far greater than the rotational period of the molecule. Another dissociation pathway for CF_4^+ is fluorescence to the lower dissociative electronic states which is also a slow process. This fluorescence has been observed in another experiment [30]. The $B1$ state-to-state transition energy is 275.5 eV which is in good agreement with the peak position of area B in Fig. 2. On the overall, this $B1$ transition gives rise to an angular distribution of fragments that should be isotropic since the CF_3^+ fragment is created hundreds of femtoseconds after the Auger decay.

In order to explain the slight anisotropy observed in area B of Fig. 2, a dissociative process faster than the rotation period must be introduced for the same range of transition energies. This $B2$ process occurs if the Auger decay target state is $CF_3^+(^{1,3}E) + F$, when the wave packet reaches the dissociative area for $R_{C-F} > 1.9$ Å or possibly R_{C-F} as small as 1.4 Å when the kinetic energy of the fragments is taken into account. The $B2$ arrow in Fig. 3 shows the states concerned in the electronic transition but effective transitions will cover a large energy interval, depending on the time at which the decay occurs. The equilibrium geometries of these CF_3^+ electronic states are not planar and no angular geometry rearrangement of this fragment has to be considered. The asymptotic electronic transition energy is approximately 272 eV in agreement with area B peak limit in Fig. 2 and Ref. [14] analysis about the dissociation limit of the $3t_2^{-1}$ electronic components of CF_4^+.

In conclusion, the fragment angular distribution patterns measured by Auger electron-photoion coincidence

measurements are very informative of the nature of intermediate and final states. Combined with theoretical calculations, such patterns can yield information on the nature of the dissociation processes and on the time scales concerned. In particular, we are able to identify three different processes labeled A, $B1$, and $B2$, leading to the same fragment, but of different nature, and with very different time scales, and therefore different angular distributions.

The authors are grateful to the staff of the UVSOR Synchrotron Facility for their support and stable operation of the storage ring during the course of the present experiment.

[1] O. Björneholm, A. Nilsson, A. Sandell, B. Hernnäs, and N. Mårtensson, Phys. Rev. Lett. **68**, 1892 (1992).
[2] O. Björneholm, S. Sundin, S. Svensson, R. R. T. Marinho, A. Naves de Brito, F. Gelmukhanov, and H. Agren, Phys. Rev. Lett. **79**, 3150 (1997).
[3] P. A. Brühwiler, O. Karis, and N. Mårtensson, Rev. Mod. Phys. **74**, 703 (2002).
[4] O. Björneholm *et al.*, Phys. Rev. Lett. **84**, 2826 (2000).
[5] R. Feifel *et al.*, Phys. Rev. Lett. **85**, 3133 (2000).
[6] I. Hjelte *et al.*, Chem. Phys. Lett. **334**, 151 (2001).
[7] L. Rosenqvist *et al.*, J. Chem. Phys. **115**, 3614 (2001).
[8] I. Hjelte, M. N. Piancastelli, C. M. Jansson, K. Wiesner, O. Björneholm, M. Bässler, S. L. Sorensen, and S. Svensson, Chem. Phys. Lett. **370**, 781 (2003).
[9] O. Travnikova *et al.*, Phys. Rev. Lett. **116**, 213001 (2016).
[10] H. Sann *et al.*, Phys. Rev. Lett. **117**, 243002 (2016).
[11] H. Aksela, S. Aksela, M. Ala-Korpela, O. P. Sairanen, M. Hotokka, G. M. Bancroft, K. H. Tan, and J. Tulkki, Phys. Rev. A **41**, 6000 (1990).
[12] A. Menzel, B. Langer, J. Viefhaus, S. B. Whitfield, and U. Becker, Chem. Phys. Lett. **258**, 265 (1996).
[13] E. Pahl, L. S. Cederbaum, H.-D. Meyer, and F. Tarantelli, Phys. Rev. Lett. **80**, 1865 (1998).
[14] M. N. Piancastelli, R. Guillemin, M. Simon, H. Iwayama, and E. Shigemasa, J. Chem. Phys. **138**, 234305 (2013).
[15] K. Ueda, M. Simon, C. Miron, N. Leclercq, R. Guillemin, P. Morin, and S. Tanaka, Phys. Rev. Lett. **83**, 3800 (1999).
[16] Y. Hikosaka and E. Shigemasa, J. Electron Spectrosc. Relat. Phenom. **152**, 29 (2006).
[17] X. Tang, X. Zhou, M. Wu, Z. Gao, S. Liu, F. Liu, X. Shan, and L. Sheng, J. Chem. Phys. **138**, 094306 (2013).
[18] T. Kaneyasu, Y. Hikosaka, and E. Shigemasa, AIP Conf. Proc. **879**, 1793 (2007).
[19] T. Kaneyasu, Y. Hikosaka, and E. Shigemasa, J. Electron Spectrosc. Relat. Phenom. **156**, 279 (2007).
[20] See Supplemental Material at http://link.aps.org/supplemental/10.1103/PhysRevLett.119.203203 for the description of theoretical details, which includes Refs. [21–27].
[21] H.-J. Werner and P. J. Knowles, J. Chem. Phys. **82**, 5053 (1985).
[22] P. J. Knowles and H.-J. Werner, Chem. Phys. Lett. **115**, 259 (1985).
[23] H.-J. Werner, P. J. Knowles, G. Knizia, F. R. Manby, M. Schütz *et al.*, MOLPRO, version 2012.1, a package of *ab initio* programs.
[24] T. H. Dunning, Jr., J. Chem. Phys. **90**, 1007 (1989).
[25] A. W. Potts, H. J. Lempka, D. G. Streets, and W. C. Price, Phil. Trans. R. Soc. A **268**, 59 (1970).
[26] A. O. Mitrushenkov, P. Palmieri, C. Puzzarini, and R. Tarroni, Mol. Phys. **98**, 1677 (2000).
[27] T. J. Park and J. C. Light, J. Chem. Phys. **85**, 5870 (1986).
[28] T. X. Carroll, K. J. Børve, L. J. Sæthre, J. D. Bozek, E. Kukk, J. A. Hahne, and T. Darrah Thomas, J. Chem. Phys. **116**, 10221 (2002).
[29] C. Léonard and F. Le Quéré, J. Chem. Phys. **137**, 164318 (2012).
[30] U. Müller, M. Lange, W. Haas, and R. Brenn, J. Chem. Phys. **100**, 5550 (1994).